Seismic Profiling of Faults Related to the 1886 Charleston Earthquake: Summerville Survey

Lee M. Liberty, Department of Geosciences, Boise State University, lliberty@boisestate.edu

Project Award Number: # G19AP00080

Award Dates: July 2019 through September 2022

Submission date: December 31, 2022

Research supported by the U.S. Geological Survey (USGS), Department of the Interior, under USGS award number G19AP00080. The views and conclusions contained in this document are those of the authors and not be interpreted as necessarily representing the official policies, either expressed or implied, of the U.S. Government.

Abstract

We acquired 9.4 km of new seismic data in the Summerville/North Charleston, South Carolina area to map active faults related to the 1886 and earlier Charleston earthquakes. We used an accelerated hammer/hand streamer seismic system along road shoulders and sidewalks of secondary roads to identify offsets or disruptions in Tertiary and younger strata. We obtained reflection images for the upper 100-200 m depth to map Tertiary stratigraphy and shear wave velocity images of the upper 5-10 m depth to map Quaternary strata. We compare these results with previously published fault maps to further constrain fault locations and displacements. Results from this study support evidence for late-Quaternary fault motion in the Charleston, South Carolina area.

Setting

Because there is no surface expression of active or dormant faults in the Charleston, South Carolina area, the locations, geometries and fault lengths of potentially active faults are poorly constrained. Because of sparse subsurface data, many under-constrained interpretations have been published. Figure 1 shows a summary of some mapped faults in the study area with new seismic profile locations. From topography and stream gradients, Marple and Talwani (1993 and 2000) mapped the East Coast fault to extend through Ravenel and Summerville regions. This fault is consistent with 1) a region of modern seismicity termed the Middleton Place-Summerville Seismic Zone (Dura-Gomez and Talwani, 2009; Chapman et al., 2016), 2) within the 1886 epicentral region (Figure 1; Dutton, 1889), and 3) an inflection and offset in seismic reflectors (Chapman and Beale, 2010; Marples and Miller, 2006). Subsequent interpretations by Talwani and Dura-Gomez (2009) revised the fault geometry and locations based on a new catalog of seismicity and structural models. They termed the Woodstock fault as the dominant structural fault in the region. This fault system includes a left step and Summerville fault connecting the two northeast-striking, right-lateral, strike-slip North and South Woodstock fault segments. However, Maple (2011) did not support this interpretation, suggesting that the Woodstock fault was indeed not offset at some locations. Other faults mapped in the region include the Adams Run fault (Weems and Lewis, 2002) to accommodate a cluster of seismicity related to other mapped structures, the Dorchester fault from Bartholemew and Rich (2007) that has not received the support of more recent papers (e.g., Talwani and Dura-Gomez, 2009), and the Magnolia faults (Pratt et al., 2022) that align offset river channels, 1886 earthquake deformation, and vertical displacements mapped from regional seismic profiles. Whereas many of the legacy seismic profiles extend through the Summerville area, none of the seismic images show reflectivity to depths shallower than about 100 m (e.g., Chapman and Beale, 2010; Pratt et al., 2022) and the resolution is not sufficient to make definitive statements about late Quaternary fault motions. This survey, and results from a previous NEHRP project (NEHRP #G17AP00040), examines many of these regional faults to determine locations and slip histories. By integrating shallow seismic images from this report with legacy seismic and new aeromagnetic data, slip history and geologic structures are better constrained for the Charleston, South Carolina region.

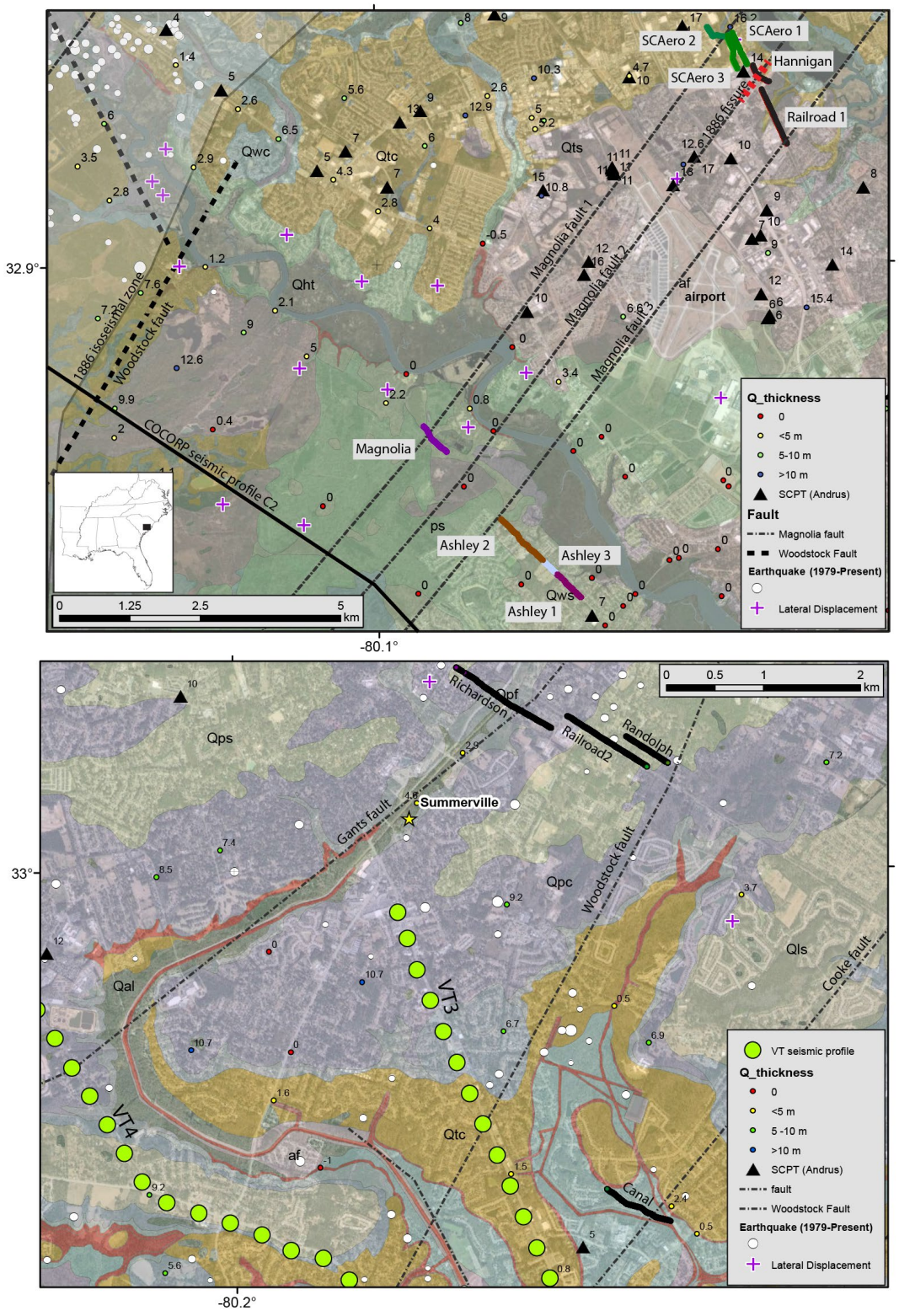

Figure 1. Study areas with geology, faults (dashed), horizontal displacement and craterlet regions from Dutton (1889), ANSS earthquake epicenters (circles), and the location of previous seismic surveys. New profiles focus on the Magnolia, Cooke, Woodstock and Gants faults. Geologic units are from Weems et al. (2014). Labels next to corehole and SCPT measurements reflect top of Tertiary depth.

Chapman et al. (2006) noted that a shallow impedance contrast between Quaternary sediments and the underlying Tertiary rock largely controls the 1-10 Hz earthquake site response and this depth estimate is an important parameter to characterize site response for the Charleston area. Within this frequency range, site response can vary by a factor of three, where Tertiary rock can be as shallow as a few meters depth or less (Figure 1). This study measured shear wave velocities (Vs) of 150-250 m/sec in the Quaternary alluvium and 300-500 m/sec in the underlying Tertiary strata. Heidari and Andrus (2012) updated this study to show beach sand, estuarine and fluvial surficial deposits are present at the 1886 ground displacement and craterlet sites. Data collection from 2018 (NEHRP #G17AP00040; Liberty, 2018) produced more than 5000 shot gathers where high quality dispersion curves were obtained. From this dataset, we utilized an MASW approach to estimate Vs to about 20 m depth, an approach where results are on par with downhole measurements (Stephenson et al., 2005). These measurements, in concert with body wave images, document the variations in Vs properties, and identify Tertiary bedrock depth and fault locations in the vicinity of extensive 1886 liquefaction and lateral displacements. This report expands the seismic database to include 18,000 new Vs measurements in the Summerville and North Charleston regions (Figure 1) and more than nine km of new reflection imagery. These results can be compared to previous downhole studies to further constrain ground motion models.

Seismic imaging approach

Seismic land streamer technology has gained support and use for the past 20+ years. Van der Veen and Green (1998) first constructed and tested land streamers with gimbaled geophones. Their interest was in rapid p-wave seismic reflection acquisition, but recognized the potential to integrate a variety of seismic source and receivers into this technology. For the past decade, other land streamer designs have been developed and used with shear wave source and receivers, hammer, weight drop, and vibroseis sources. Boise State land streamers were first developed with EHP funds (#G13AP00032) to develop one-, two-, and three-component systems that rapidly and accurately operate on city streets. Weight drop operations on city streets and other paths have been used for the past 15 years at Boise State and signal processing approaches to dealing with urban noise have been developed (Liberty, 2011). Integrated with computer controlled accelerated hammer sources, we simultaneously record body wave and surface wave signals (Figure 2) to obtain detailed images beneath urbanized regions (Gribler et al., 2016; Liberty et al. 2021). With our current field approach, all operations are performed by a single person, while the other members of the field team interact with motorists, residents and the streamer. For this survey, we collected a shot gather every 0.5 meters to obtain profiles at a rate of about 200 m/hour or about 1.5 to 2 km/day. We operated during normal business hours on quiet streets and sidewalks to optimize signal quality. From the field records (Figure 2), we automatically extract Rayleigh wave signals to obtain Vs profiles to estimate subsurface elastic (soil stiffness) conditions. This approach is similar to MASW (Park et al., 1999; Xia et al., 1999), where we use a smooth layer inversion approach to best-fit the peak semblance of Rayleigh wave phase velocities for a range of frequencies (Lai and Rix, 1998; Liberty, 2020; Liberty et al., 2021). We infer lithology from previous borehole and surface studies (e.g., Weems et al., 1987; Andrus et al., 2006) and we map stratigraphy using the reflected signals to locate/characterize active faults. We use the standard reflection processing approach of Yilmaz (1987) to produce final stacked images. We convert travel time to depth assuming 1500 m/s, consistent with downhole and previous seismic imaging approaches for the region. We present only unmigrated seismic images.

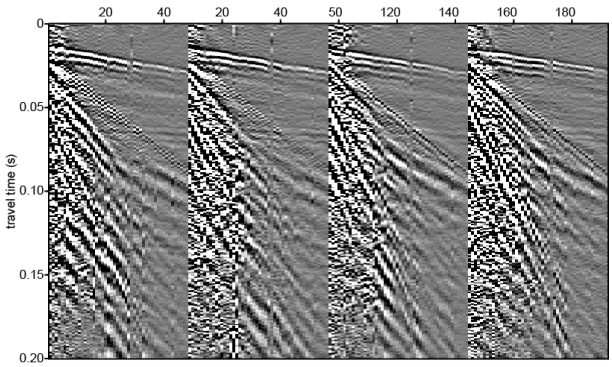

Figure 2 (left). Hand streamer acquisition system. Electric hammer is controlled by the operator of the cart (button on handle). The 0.5 m spaced, 48 channel, 40 Hz geophone streamer was located ~5 m behind the source to allow for reflection and surface wave returns. A noise blanket surrounds the source to reduce air-coupled signals. The geophone data are digitized with two 24-channel Geode recording systems and stored on a field laptop. (below) Example field gathers showing first arrivals, surface waves and reflections that are generated from the electric hammer/hand streamer system. Note that the prominent reflection at about 0.07 s (~50 m depth) extends into the surface wave window, allowing for reflection imaging to depths up to 200 m. Dispersion images show unconsolidated sediments (~150 m/s) and shallow bedrock (phase velocities ~400 m/s) along each profile. These gathers were from the Magnolia profile. Red circles depict fundamental mode autopicks.

Seismic Results

Magnolia profile

We acquired the ~600 m long west to east Magnolia seismic profile along an access road of the Magnolia Plantation adjacent to Ashley River Road (Figure 1). This profile was acquired along gravel and paved roads and crosses the projected location of Magnolia fault 1 (MF1) near position 6800 (Pratt et al., 2022). A low fold region from crossing the entrance to the heavily trafficked plantation tour access road resulted in poor reflection data quality near the projected fault location, but Rayleigh wave data coverage was adequate to obtain a robust Vs profile to 5+ m depth (Figure 3). Reflectivity appears to more than 100 m depth.

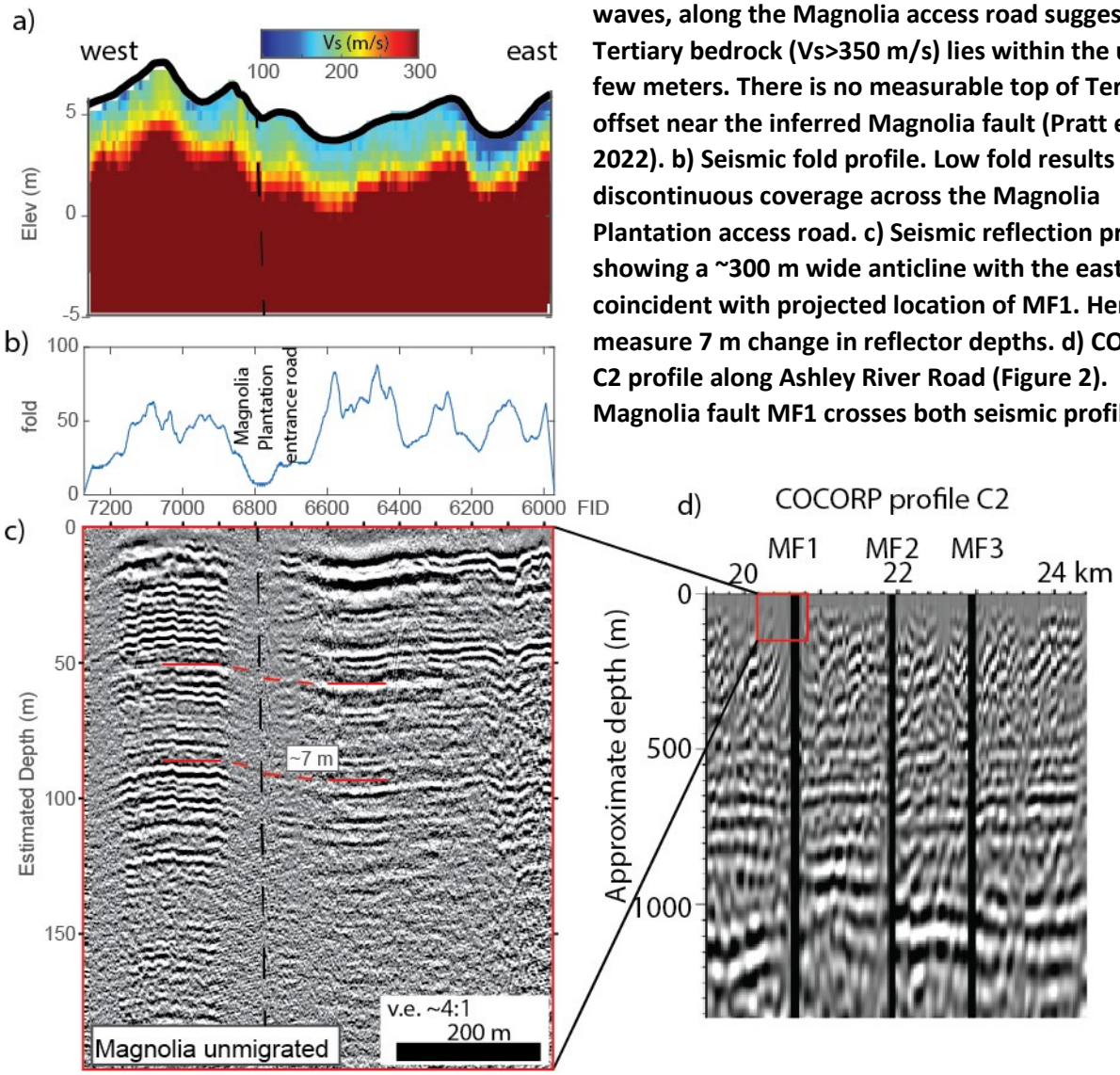

Figure 3. a). Vs profile, derived from Rayleigh waves, along the Magnolia access road suggests Tertiary bedrock (Vs>350 m/s) lies within the upper few meters. There is no measurable top of Tertiary offset near the inferred Magnolia fault (Pratt et al., 2022). b) Seismic fold profile. Low fold results from discontinuous coverage across the Magnolia Plantation access road. c) Seismic reflection profile showing a ~300 m wide anticline with the east limb coincident with projected location of MF1. Here, we measure 7 m change in reflector depths. d) COCORP C2 profile along Ashley River Road (Figure 2). Magnolia fault MF1 crosses both seismic profiles.

The Magnolia Vs profile shows Rayleigh wave speeds less than 200 m/s above about 20 Hz (Figure 3). At lower frequencies, the phase velocities increase to about 400 m/s (Figure 2). An inversion of the Rayleigh waves suggests an abrupt velocity boundary about two to four meters below the ground surface. This Vs increase from ~160 m/s to ~400 m/s is consistent with a transition from unconsolidated Quaternary strata to Tertiary strata. This boundary depth is consistent with shallow top of Tertiary values from downhole core and SCPT measurements (Weems et al. 1987, Andrus et al, 2006; Figure 1). Vs <120 m/s lies beneath a topographic low near the eastern margin of the profile. We interpret this slow zone as a modern fluvial channel. Low elevations and a nearby swamp and river suggest water saturated sediments lie within a few meter of the land surface.

Seismic reflection results suggest near flat-lying strata along much of the profile, with a broad ~300 m warp between positions 6800 to 7200 (Figure 3). Reflectors map down to the east with an offset estimated at about seven meters (assuming 1500 m/s sediment velocity) near position 6800. Although the location of the offset is coincident with the MF1 fault mapped by Pratt et al (2022), the sense of motion is not consistent with offset on deeper reflectors on COCORP profile C2. This offset pattern may suggest dominantly strike-slip fault motion along this strand of the Magnolia fault, with little dip-slip motion. From our Rayleigh wave inversions, there does not appear to be significant vertical offset or lateral Vs change in the upper few meters at the fault location, consistent with little Quaternary deformation or vertical motion on this fault strand.

Ashley Bike Path profiles

The Ashley bike path consisted of three seismic profiles that span 2+ km. These northwest to southeast oriented profiles are located to the southeast of the Magnolia faults as mapped by Pratt et al. (2022) (Figure 1). Access restrictions along an unshouldered busy highway prevented an extension of these profiles to the northwest where other strands of the Magnolia fault system was mapped. The surface elevation changes by upwards of four meters, with a large hill along the Ashley2 profile. Seismic profile COCORP C2 was located along Ashley River Road adjacent to the bike path, and this profile highlights stratigraphy to depths upwards of one km (e.g., Pratt et al., 2022; Figure 1; Figure 4).

Vs profiles derived from Rayleigh wave inversions suggest Tertiary strata lies about two meters below land surface along the western 300 m and between position 900 to 1000 m of the Ashley2 profile (Figure 4). Vs at similar depths decreases at all other locations, consistent with a greater thickness of Quaternary strata. Corehole and SCPT data show depths from zero to seven meters in the vicinity of the Ashley transect (Figure 1), consistent with these new measurements. The abrupt change in Vs at 5+ m depth at position 300 m distance on Ashley 2 may be fault related.

Seismic reflection profiles show near flat-lying strata to 100+ m depth (Figure 4). Data quality was highly variable along this transect, limiting reflection interpretations along Ashley1 and Ashley3 profiles. Pratt et al (2022) showed no clear evidence for offset along deeper reflectors, consistent with limited deformation to the east of the mapped Magnolia faults. However, the Ashley2 profile shows indications of fault offsets to the shallowest reflectors. In particular, the large lateral Vs change at position 300 m matches a down to the southeast step in reflectors, consistent with post Wando Formation (70-130 ka) deformation (Weems et al., 2014; Figure 1). A zone of offset reflectors extends to position 820 m, suggesting a ~500 m wide deformation zone on Ashley2. This includes a ~9 m up to the southeast step near position 700 m. Although there is low resolution and position uncertainties with COCORP C2, the faults identified along profile Ashley2 match the deeper deformation style interpreted

by Pratt et al (2022) for Magnolia fault 3. Offset of the shallowest reflector and an abrupt lateral changes in shallow Vs along the Ashley2 show compelling evidence for late Quaternary faulting.

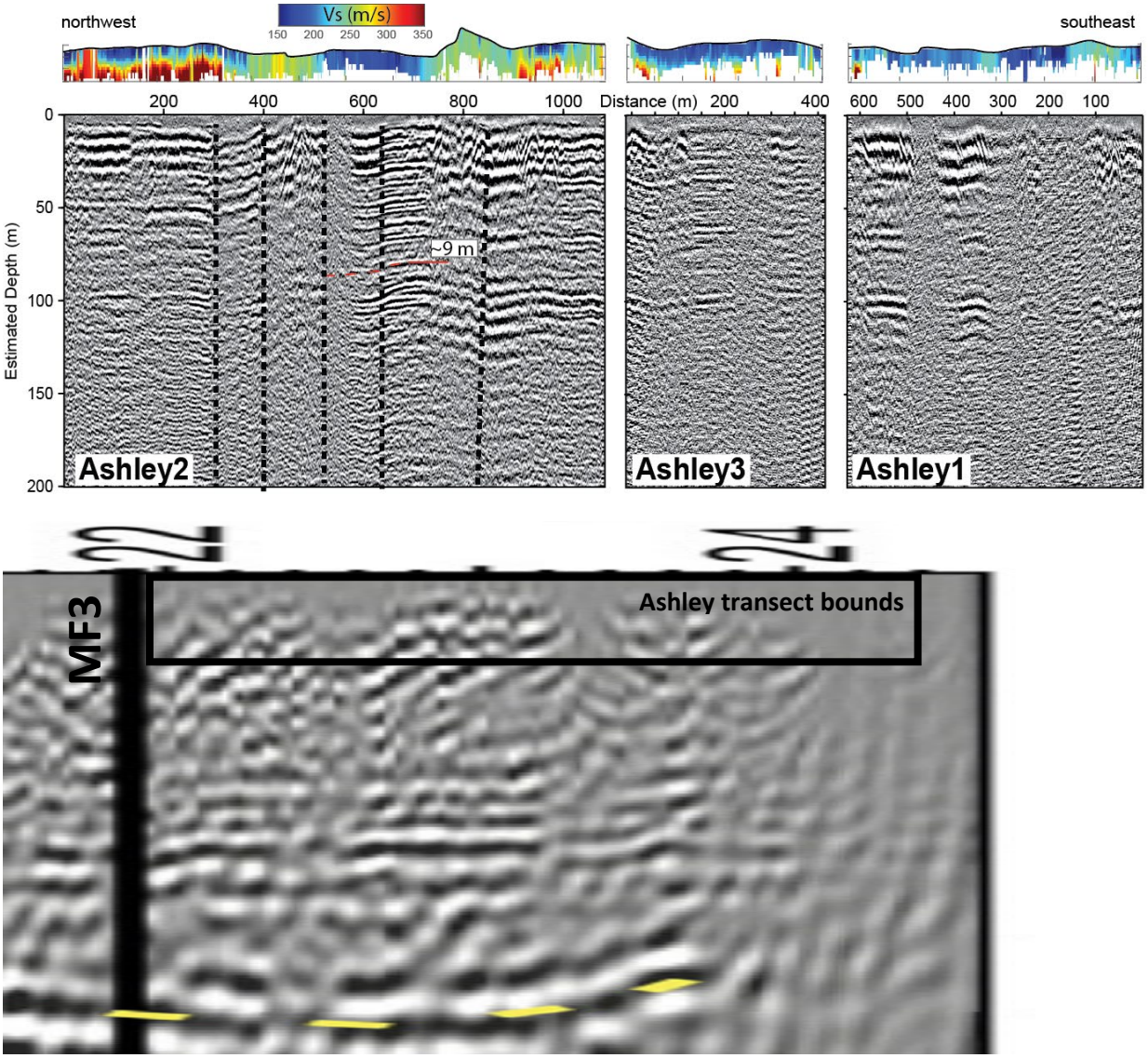

Figure 4. (top) Vs profile, derived from Rayleigh waves, along the Ashley bike path transect. Vs>400 m/s appears in the upper few meters along the western portion of the transect, consistent with shallow Tertiary strata. Farther east, Vs<200 m/s extends across the transect, consistent with greater depths to Tertiary strata. (middle) seismic reflection profile from the hand streamer showing undulating stratigraphy in the upper 100 m of the transect. While there is no clear evidence for a faulted section, shallow offsets may be present. (bottom) COCORP C2 profile along Ashley River Road (Figure 2) with black box showing location of the Ashley transect. Seismic profile C2 from Pratt et al. (2022). MF3=Magnolia fault 3 as shown on Figure 1.

Hannihan/Railroad1 profiles

We acquired the 420 meter-long northwest to southeast Hannihan seismic profile along a parking lot and sidewalk associated with the Hannihan city park (Figure 1). There was about a two-meter elevation change along this profile with a bend in the profile near position 200 meters. We acquired the adjacent and parallel 1100 meter-long Railroad1 profile along a sidewalk that paralleled the main rail line where Dutton (1889) identified deformation during the 1886 earthquake. This profile crosses a stream near position 300 m, with a total elevation change of about 4 m. Andrus et al. (2006) identified Tertiary-age Cooper Marl close to the northwest end of the Hannihan profile at a depth of 14 m (Figures 1 and 5).

Our Vs profiles obtained from Rayleigh wave data show Vs<250 m/s along the length of each profile, consistent with Quaternary-age unconsolidated sediments in the upper 3-5 meters (Figure 5). This observation is consistent with nearby CPT boreholes that suggest Tertiary strata lie >10 m below ground surface (Andrus et al., 2006; Figure 1). We note that the lower elevation regions record lower Vs values, consistent with Holocene sediments occupying the floodplains a few meters above sea level. At position 220 m of the Hannihan profile, we note a 50 m/s decrease in Vs to the southeast. A similar lateral change in Vs is noted near positions 600 m, 780 m, and 1000 m along the Railroad1 profile.

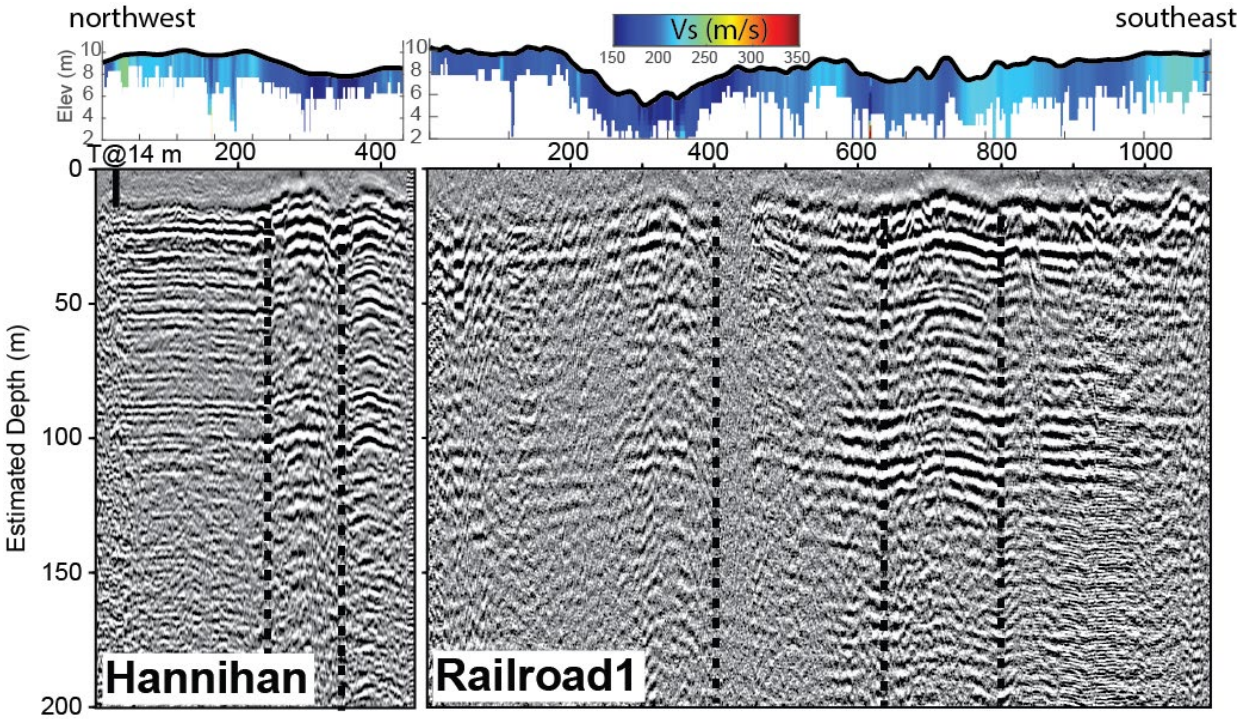

Figure 5. Hannigan/Railroad1 seismic transect. Vs and borehole data suggest depth to top of Tertiary strata lies >10 m depth. Seismic reflection profiles show offset and tilted reflectors suggesting post-depositional fault deformation. Railroad deformation in the region suggests Holocene fault motion.

The Hannihan seismic reflection profile shows flat-lying strata below about 15 m depth between positions 0 to 220 m distance (Figure 5). This top of reflectivity is consistent with top of Tertiary-age Cooper Marl (Weems et al., 1987; Andrus et al. 2006). To the southeast of position 220 m distance, we note an undulating and offset reflectors. This location is consistent with 1886 deformation observed along nearby Railroad tracks (Dutton, 1889; Pratt et al., 2022) and suggests up to the southeast fault offsets of a few meters. Railroad1 profile contains gently undulating reflectors that suggests folds and faults. The most abrupt reflector offset is located near position 400 m, with a change in reflector dip to the southeast and northwest. A gentle antiformal fold is centered near position 700 m, with fold axes spaced about 80 m to the southeast and northwest. These reflector offsets and deformation zone is consistent with additional fault strands related to the northeast-trending Magnolia fault system, as mapped by Pratt et al., (2022) (Figure 1). Lateral changes in shallow Vs at these fault locations suggests that deformation may post-date the 200-240 ka Ten Mile Hill strata that are mapped at the surface (Weems et al., 2014; Figure 1).

SC_Aero profiles

Three seismic profiles were acquired near the Trident Technical College Building 1000, approximately one km to the north of the Hannihan/Railroad1 transect. The profiles surround the buildings associated with aeronautical studies and here named the SC_Aero transect. SC_Aero1 and SC_Aero3 are parallel south to north profiles that straddle the main campus building (Figure 1). These profiles vary in surface elevation by about two meters. SC_Aero2 profile extends from the north portion of campus north to the Walmart parking lot. This profile crosses a broad drainage that changes in elevation by about 5 meters. Pratt et al (2022) mapped the Magnolia fault extending through this transect (Figure 1).

The Vs profiles, derived from Rayleigh waves, show mostly Vs<250 m/s (Figure 6). These low velocities are consistent with Quaternary strata in the upper few meters below land surface (Figure 6). Vs values <150 m/s occupy the lowest elevations, consistent with Holocene deposits at elevations close to sea level (Andrus et al., 2006). Nearby auger data are consistent with our Vs results, where depth to top of Tertiary strata is greater than 10 m (Figure 1).

Seismic reflection results show mostly flat-lying or broadly folded strata along SC_Aero1 and SC_Aero3 profiles with a ~5 m up to the north step on each profile that, if connected, is consistent with a northeast-trending fault (Figures 1 and 6). Profile SC_Aero2 shows significant reflector offsets near distance 300 m, consistent with an up to the north fault within the low elevation region of the profile. The ~50 m wide deformation zone to the north is consistent with some compressional fault dip-slip motion. These faults are within the Magnolia fault system of Pratt et al (2022) and are consistent with the location of railroad deformation related to the 1886 earthquake (Dutton, 1889). Offset of the shallowest reflectors suggest Quaternary fault motion.

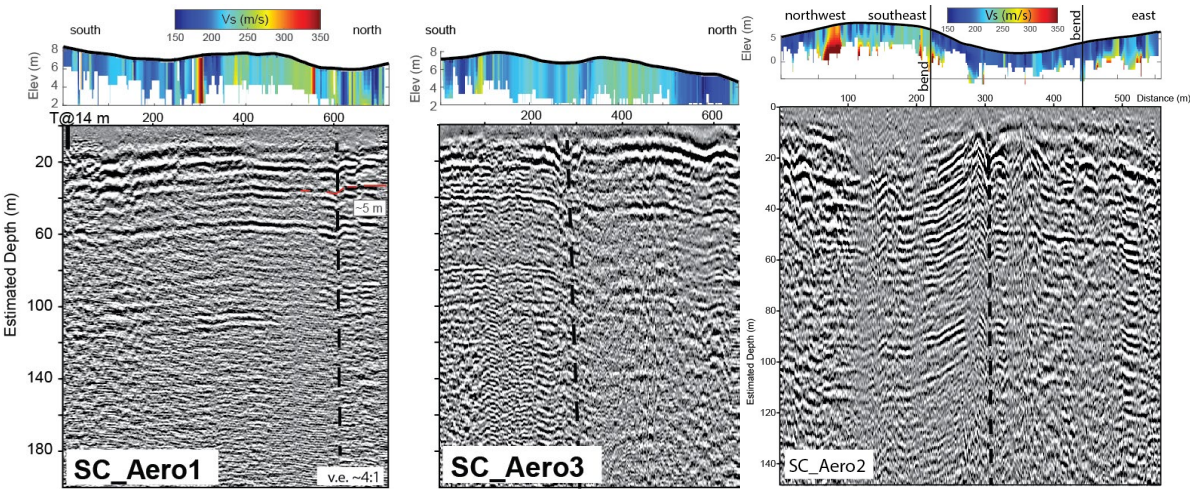

Figure 6. SC_Aero seismic profiles showing Vs<250 m/s, consistent with Quaternary strata in the upper 5 meters. Reflection images show gently folded strata with offset reflectors on all three profiles. These offsets are consistent with strands of the Magnolia fault system.

Summerville region

Richardson/Railroad2 transect

The ~2 km long Richardson/Railroad2 transect is located near the town of Summerville and crosses near the mapped location of the Gants and Woodstock faults (Figure 1). The 1200 m long Richardson profile along County road S-10-65, extends east from Owens Road, west across the Sawmill Branch trail and canal, and ends at South Main Street in Summerville. The surface elevation changes by about 9 meters, with the lowest elevation at the river level of the Sawmill Branch. The ~1000 m long Railroad2 profile extends west from Owens Road, east to termination along Railroad Avenue at Pinckney Street. This profile changes elevation by about 5 meters, with the highest elevation near the profiles' center. The projection of the Gants and Woodstock faults across this transect region were previously mapped from geomorphic features (Marple and Talwani, 1993) and seismic imagery (e.g., Pratt et al., 2022).

The Rayleigh waves suggest Vs<250 m/s along the length of the transect to a depth of ~5 m below land surface (Figure 7). Higher Vs values are noted in the center of the Railroad2 profile, but these values lie near the maximum resolvable depth from Rayleigh waves. There are no shallow auger or SCPT profiles in the region to confirm this observation.

Seismic reflection results show large lateral changes in reflector depths along the Richardson profile, consistent with two or more faults to the east of the Sawmill Branch. This location coincides with the mapped location of the Gants fault from seismic and topographic data. An antiformal fold centered near position 800 m may also be fault controlled, and the tilted strata that extend beyond the southeast limits of this profile are consistent with additional faults within this region. The reflection results from the Railroad2 profile suggests a broad fold between lies between two small offset faults. These faults lie to the northwest of the mapped Woodstock fault and to the southeast of the Gants fault (Figure 1). Tilted strata along the northwest and southeast limits of this profile suggest additional faults may

control the structural style of the region. Pratt et al (2022) mapped this area as a ~2.5 km wide faulted region, consistent with our new seismic data results.

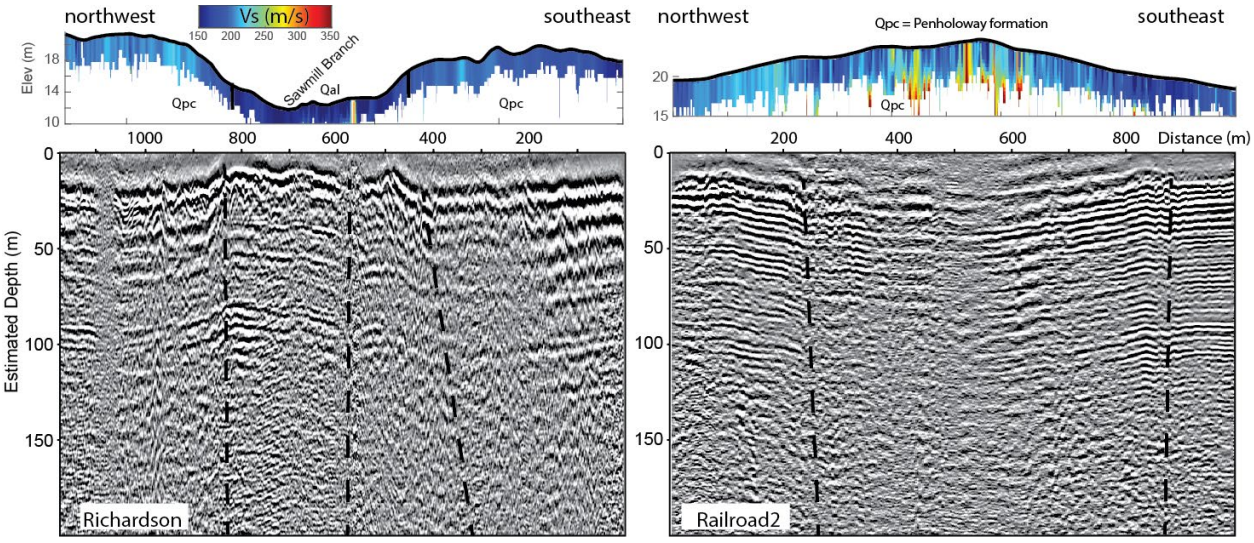

Figure 7. Richardson and Railroad2 seismic profiles showing Vs<250 m/s, consistent with Quaternary strata in the upper 5 meters. Reflection images show folded strata with offset reflectors on both profiles. These offsets are consistent with strands of the Gants and Woodstock faults.

Canal profile

The Canal seismic profile crosses the Cooke fault (Figure 1), and extends along a footpath and residential road parallel to Chandler Bridge Creek. Along the river bank, near the eastern limits of the seismic profile, southeast-dipping and offset strata are visible in outcrop. The profile gently changes in elevation by a few meters. The fault has been mapped by a number of studies and is summarized in Pratt et al. (2022).

The Rayleigh wave speeds are consistent with Vs>350 m/s along much of the profile, suggesting shallow Tertiary strata (Figure 8). A nearby corehole places Tertiary strata at about 2 m below land surface (Weems et al., 1987; Figure 1). At positions less than ~50 m, we observe Vs<200 m/s, transitioning to Vs>350 m/s farther to the northwest. This is close to the mapped location of the Cooke fault, and we interpret 5+m of Quaternary strata adjacent to Tertiary strata. If this lateral change in Vs is fault controlled, it suggests post 200-700 ka Ladson formation deformation (Figure 1).

Although the seismic reflection data are not high quality, broad folding and offset reflectors suggest a deformation zone that is consistent with offsets associated with the Cooke fault. Detailed interpretation of this reflection profile is not warrented, based on the poor imagery.

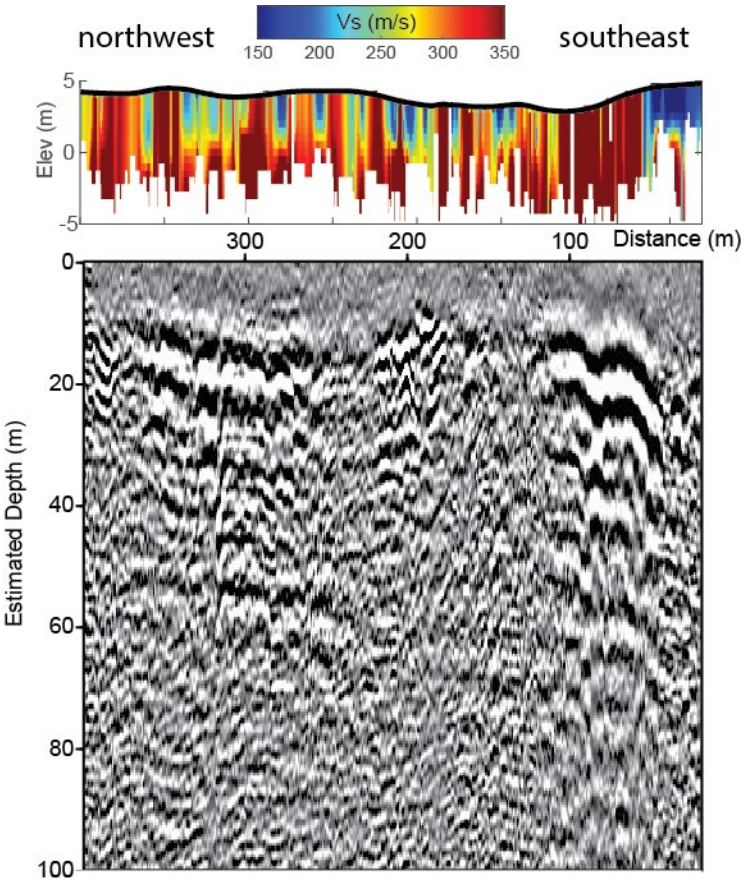

Figure 8. Canal seismic profile showing mostly Vs>250 m/s, consistent with Tertiary strata in the upper 5 meters. The exception is along distance 0-50 m, where slower Vs is consistent with shallow Quaternary (Ladson formation) strata. Reflection image suggests folded Tertiary strata. It is unclear whether faults bound these folds.

Summary

New seismic data in the vicinity of the 1886 Charleston earthquake epicenter show evidence for late Quaternary fault motion. We observe offset of the shallowest reflectors (<10 m depth) and large lateral changes in shear wave velocities in the upper few meters that may point to latest Quaternary fault motion of deformation. Given the location of craterlets and liquefaction noted during the 1886 earthquake (Dutton, 1889), these faults may be active. We suggest that trenching of these sites may confirm recent fault motion.

Data availability

The seismic data acquired for this project will be compiled as an IRIS assembled data product.

References

Andrus, R. D., Fairbanks, C. D., Zhang, J., Camp III, W. M., Casey, T. J., Cleary, T. J., & Wright, W. B. (2006). Shear-wave velocity and seismic response of near-surface sediments in Charleston, South Carolina. *Bulletin of the Seismological Society of America*, 96(5), 1897-1914.

Bartholomew, M. J., and Rich, F. J. (2007). The walls of colonial Fort Dorchester: A record of structures caused by the August 31, 1886 Charleston, South Carolina earthquake and its subsequent earthquake history. Southeastern Geology, 44(4), 147-169.

Chapman, M. C., and Beale, J. N. (2010). On the geologic structure at the epicenter of the 1886 Charleston, South Carolina, earthquake. Bulletin of the Seismological Society of America, 100(3), 1010-1030.

Chapman, M. C., Beale, J. N., Hardy, A. C., and Wu, Q. (2016). Modern Seismicity and the Fault Responsible for the 1886 Charleston, South Carolina, Earthquake. Bulletin of the Seismological Society of America, 106(2), 364-372.

Chapman, M. C., Martin, J. R., Olgun, C. G., & Beale, J. N. (2006). Site-response models for Charleston, South Carolina, and vicinity developed from shallow geotechnical investigations. Bulletin of the Seismological Society of America, 96(2), 467-489.

Durá-Gómez, I., and P. Talwani (2009). Finding faults in the Charleston area, South Carolina: 1. Seismological data, *Seismol. Res. Lett.* 80, 883–900, doi: 10.1785/gssrl.80.5.883.

Dutton, C. E. (1889). The Charleston earthquake of August 31, 1886, in Ninth Annual Report of the U.S. Geological Survey to the Secretary of the Interior, J.W. Powell, Director, U.S. Geological Survey, Department of the Interior, U.S. Government Printing Office, Washington, D.C., 203–528.

Gribler, G., Liberty, L. M., Mikesell, T. D., & Michaels, P. (2016). Isolating retrograde and prograde Rayleigh-wave modes using a polarity mute. *Geophysics*, *81*(5), V379-V385

Heidari, T., and R. D. Andrus (2012). Liquefaction potential assessment of Pleistocene beach sands near Charleston, South Carolina, *J. Geotech. Geoenviron. Eng*. 138, 1196–1208, doi: 10.1061/(ASCE) GT.1943-5606.0000686.

Lai, C. G. and Rix, G. (1998). Simultaneous inversion of Rayleigh phase velocity and attenuation for near-surface site characterization. Georgia Institute of Technology.

Liberty, L.M. (2021). Hammer seismic reflection imaging in an urban environment, The Leading Edge, v. 30, no. 2, doi:10.1190/1.3555324.

Liberty, L. M. (2018). Seismic profiling of faults related to the 1886 Charleston, South Carolina earthquake: A collaborative US Geological Survey project: USGS NEHRP final technical report G17AP00040.

Liberty, L. M., St. Clair, J., & McKean, A. P. (2021). A Broad, Distributed Active Fault Zone Lies beneath Salt Lake City, Utah. *The Seismic Record*, *1*(1), 35-45.

Liberty, L. M., St. Clair, J., Mikesell, T. D., & Schermerhorn, W. D. (2021). Resonant Frequency Derived from the Rayleigh-Wave Dispersion Image: The High-Impedance Boundary Problem. *Bulletin of the Seismological Society of America*, 111(1), 77-86.

Marple, R. T., and P. Talwani (1993). Evidence of possible tectonic upwarping along the South Carolina Coastal Plain from an examination of river morphology and elevation data, *Geology* 21, no. 7, 651–654.

Marple, R. T., and P. Talwani (2000). Evidence for a buried fault system in the Coastal Plain of the Carolinas and Virginia— Implications for neotectonics in the southeastern United States, *Geol. Soc. Am. Bull*. 112, no. 2, 200–220.

Marple, R. (2011). Comment on the Companion Articles "Finding Faults in the Charleston Area, South Carolina: 1. Seismological Data" by I. Durá-Gómez and P. Talwani and "Finding Faults in the Charleston Area, South Carolina: 2. Complementary Data" by P. Talwani and I. Durá-Gómez. *Seismological Research Letters*, 82(4), 599-605.

Marple, R. T., and R. Miller (2006). Association of the 1886 Charleston, South Carolina, earthquake and seismicity near Summerville with a 12° bend in the East Coast fault system and triple-fault junctions. Southeastern Geology 44 (3), 101–128.

Park, C.B., Miller, R.D., and Xia, J., 1999, Multichannel analysis of surface waves, *Geophysics*, 64, 800–808.

Pratt, T. L., Shah, A. K., Counts, R. C., Horton Jr, J. W., & Chapman, M. C. (2022). Shallow Faulting and Folding in the Epicentral Area of the 1886 Charleston, South Carolina, Earthquake. *Bulletin of the Seismological Society of America*, 112(4), 2097-2123.

Stephenson, W.J., Louie, J.N., Pullammanappallil, S., Williams, R.A., and Odum, J.K., 2005, Blind shear-wave velocity comparison of ReMi, and MASW results with boreholes to 200 m in the Santa Clara Valley: Implications for Earthquake Ground Motion Assessment, *Bulletin Seismological Society of America*, v. 95, n. 6, p. 2506-2516.

Talwani, P., and Durá-Gómez, I. (2009). Finding faults in the Charleston area, South Carolina: 2. Complementary data. *Seismological Research Letters*, 80(5), 901-919.

Van der Veen, M. and Green, A.G. (1998). Land streamer for shallow data acquisition: evaluation of gimbal-mounted geophones. Geophysics, 63, 1408-1413.

Weems, R. E., E. M. Lemon Jr., G. S. Gohn, and B. B. Houser (1987). Detailed sections from auger holes and outcrops in the Clubhouse Crossroads, Johns Island, Osborn, and Ravenel quadrangles, South Carolina, *U.S. Geol. Surv. Open-File Rept.* 87-661, 159 pp., doi: 10.3133/ofr87661.

Weems, R. E., and W. C. Lewis (2002). Structural and tectonic setting of the Charleston, South Carolina, region: Evidence from the Tertiary stratigraphic record, Geol. Soc. Am. Bull. 114, 24–42.

Weems, R. E., W. C. Lewis, and E. M. Lemon Jr. (2014). Surficial geologic map of the Charleston, region, Berkeley, Charleston, Colleton, Dorchester, and Georgetown Counties, South Carolina, *U.S. Geol. Surv. Open-File Rept.* 2013-1030, scale 1:100,000, 1 sheet, doi: 10.3133/ofr20131030.

Xia, J., Miller, R.D., and Park, C.B., 1999, Estimation of near surface shear-wave velocity by inversion of Rayleigh waves, *Geophysics*, 64, 691–700.

Yilmaz, O. (1987). Seismic data processing: Soc. Expl. Geophys, 252.